A Road-Holding Index Based on Ride Dynamics for High-Downforce Racing Cars

IOP Conf. Series: Materials Science and Engineering **538** (2019) 012069 doi:10.1088/1757-899X/538/1/012069

A Road-Holding Index Based on Ride Dynamics for High-Downforce Racing Cars

Felipe Marchesin[1], Roberto Spinola Barbosa[1], Marco Gadola[2,a] and Daniel Chindamo[2]

[1]Department of Mechanical Engineering, University of Sao Paulo, Sao Paulo, Brazil.
[2]Department of Industrial and Mechanical Engineering, Automotive Group, University of Brescia, I-25123 Brescia, Italy.

[a] Corresponding author: marco.gadola@unibs.it

Abstract. This work builds on some of the current industry techniques used in racing to evaluate vertical dynamics performance and propose a new methodology to evaluate vehicle performance. The proposed method creates a quantitative numerical index from the classic tyre vertical load variation frequency response function with some novelties that cover all peculiarities of high downforce race cars. In this method the aerodynamic forces are included as non-linear functions vs ride height and it is shown that they affect system stiffness and damping. As a result, the system response changes as a function of vehicle longitudinal speed. The importance of non-linear suspension rates in this kind of vehicle is also highlighted. The proposed index can also be customized for a certain vehicle speed range. A Formula 3 racecar model has been used as an application example.

1. Introduction

Since the early era of motor racing, race car dynamics has been studied by adopting a similar approach used for road cars. In the past race cars were usually derived from road cars, but since the early sixties they followed different design and development paths quite often. Road cars are designed for everyday use, customer comfort, fuel economy, reduced environmental impact etc. Race cars are designed to be as fast as possible under a set of given regulations. As a matter of fact, aerodynamics became a key performance factor in the late sixties: downforce can increase cornering speed and reduce lap time, while road car aerodynamics, in most cases, is aimed at decreasing drag to improve fuel efficiency [1]. The aerodynamic devices used in race cars, such as wings and diffusers, are not applied on road cars (except for special, high-performance road cars) as the applications have different aims, as highlighted above. Therefore, the impact of aerodynamics in terms of maximum lateral acceleration developed by a road car is usually small (values are around 0.9g) while a race car can even reach 5g [2].
With regard to vehicle mass, the minimum weight is usually given by the regulatory structure in motorsport, while weight reduction is seen as a key to sustainable mobility as far as road vehicles are concerned [3-5].
From the point of view of vertical dynamics, road car designers must achieve a compromise between comfort, road holding and stability, while race car engineers mainly focus on road holding alone. Apart from the different goals, some other characteristics are very different in magnitude. According to the authors experience and public data [6], the typical race car weight can be around 50% to 70% of

a typical road car, the centre of gravity height is around 50% lower, the ground clearance is around 25mm, and the tyres feature completely different functional characteristics. Race car tyre vertical stiffness is about the same of the suspension system (or even softer), and the presence of wings and diffusers generates high values of aerodynamic downforce. Of all differences, the most important one is aerodynamics: race car dynamics is heavily speed dependent as this work will show and discuss.
In terms of vertical dynamics, road holding can be translated into tyre contact patch load variation. The longitudinal and lateral forces available from the tyres are proportional to vertical load. Any suspension oscillation will result into fluctuation of the contact patch load that will affect vehicle performance [7, 8].
As far as vertical dynamics is concerned, several works can be found in literature on both road and racing vehicles or motorcycles. Many of them are focused on the vehicle response as function of the road input [9, 10] or on the calibration of active suspension systems [11, 12]. Benini et al. [13] investigated the influence of the suspension components friction on vertical dynamics of a race car. Studies based on the search for natural frequencies and analysis for noise, vibration and harshness (NVH) purposes can also be found [14]. Vertical dynamics can also affect cornering response in general [15, 16], torque side distribution and yaw moment if the vehicle is fitted with a limited-slip differential or a torque vectoring system [17].
A research was carried out at Clemson University coupling race car vertical dynamics and aerodynamics using a quasi-steady state approach for aerodynamics [18, 19]. The researchers' work on race car damper settings was based on frequency response and damping for different vehicle speed values. They showed that indoor testing can be replicated by simulation, thus accelerating the optimization process. They also showed that aerodynamic forces can cause instability as they affect overall stiffness and damping.
The authors developed a novel method to evaluate aerodynamic performance in high downforce race cars [20]. The impact of aerodynamic forces as non-linear functions of ride heights on lap time performance is dealt with in [21]. A work analysing aerodynamic effects on ride comfort and road holding was also published, the aerodynamic forces were non-linear functions of the ride height, but the suspension stiffness was linear [22].

1.1. Seven-post rig testing: Time domain and frequency domain approach

The four-post rig is the main indoor testing facility used to tune vertical dynamics. Basically, the four wheels are resting each on a hydraulic actuator. The system replicates the road profile applying force or position inputs to each tyre contact patch. Lateral and longitudinal accelerations are neglected in this case. However, three extra actuators can also be attached to the sprung mass to replicate aerodynamic loads and lateral load transfer. In this case the system is called seven-post rig [2] and it is mainly used for high-downforce racecars. Some works were published with time and frequency domain procedures applied to four/seven-post rigs [23, 24]. The influence of aerodynamic stability on vertical dynamics was also studied by plotting the system roots of a linearized vehicle model, trying to replicate seven-post rig testing [25].
The four- and seven-post rigs allow for time domain simulations to be performed on the vehicle using real-world road profiles. In this case, to create a suitable signal, the so-called Iterative Control System (ICS) can be used: it is an energy-based iterative process that computes an equivalent road input time history starting from suspension displacement and/or unsprung mass acceleration data recorded on a real vehicle running on a relevant road surface [9, 26].
The replication process for a high-performance racing car normally requires at least eight ICS iterations to achieve proper fitting of a full race course lap [26]. A similar method is also used by MTS [27], although [28] shows that even if the four unsprung mass vertical accelerations from the uprights can be replicated, it doesn't mean that the road profile is accurately replicated.
Several racing series are limited in terms of the maximum number of on-board data acquisition channels during official events to control costs, hence it is difficult to have access to a car with all channels required to replicate the track profile. In such a case a frequency domain-based approach can

be adopted, trying to optimize vehicle performance by means of stochastic theory. An artificial profile signal like a step or a constant velocity sine sweep can be used for basic response analysis. The vertical displacement inputs are applied in phase on the four wheels. According to some works, performance improvements can be achieved when pitch response is minimized for a certain bounce input, regardless of the type of racing car: from high-downforce formula cars to Nascar-type cars [24, 28].

In these tests, steady-state aerodynamic forces can be simulated by means of low-pressure air spring actuators (featuring near-zero stiffness and damping) applying equivalent downforce to the sprung mass. The correct car attitude is achieved by keeping suspension displacement at the correct position. Therefore, suspension kinematic properties like a variable motion ratio are considered automatically. Usually additional components giving strongly non-linear suspension rates (bump stops for instance) are removed for this kind of test [28]. It makes sense as the frequency domain approach is a linear system tool. However, the test result is often an "optimum" setup that cannot be used for impracticality, as a highly non-linear suspension rate is necessary to prevent vehicle bottoming at high speed and/or to improve aerodynamic efficiency.

The interaction between aerodynamic forces and the suspension system can be studied in two different situations: quasi-static and transient. The quasi-static analysis is mainly used to set spring stiffness, static ride heights and bump stop setup; the target is full control of ground clearance, vehicle attitude and aero balance (i.e. percentage of total downforce on the front axle) keeping them within the desired range along the whole circuit. The transient analysis is mainly used for damper setting [27].

Some authors [24, 25, 28, 29] prefer frequency domain to time domain tests. According to them the time domain approach is situation based and the track profile generated is only compatible with the related system settings. If it is modified, the system response also changes: that input profile is not realistic anymore, and it cannot be used for system optimization.

In order to make indoor testing efficient, a performance index can be adopted as a reference for each parameter to be evaluated. Typical performance indexes are listed below for a frequency domain analysis based on a sine sweep input [30]:

- Bounce and pitch coupling factor to be minimized, targeting a pitch gain reduction to improve both mechanical and aerodynamic balance;
- Front and rear ride height stability, translating into aerodynamic stability;
- Wheel load variation for both front and rear axles, to be minimized for maximum grip;
- Ratio between tyre and suspension deflection as an indicator for tyre temperature gain due to hysteresis;
- Heat energy absorbed by tyres, again as an indicator for tyre temperature.

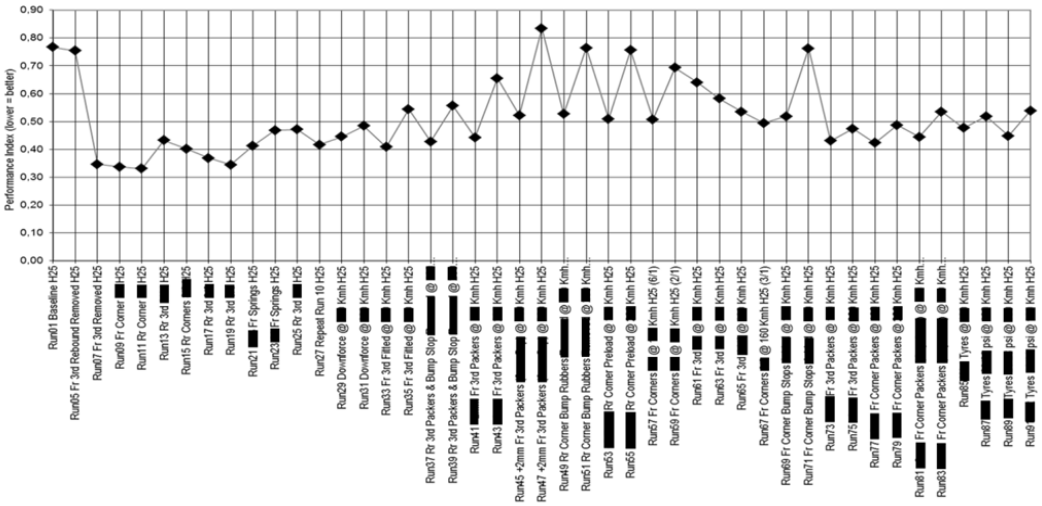

Figure 1. Performance index evolution in a series of frequency domain tests (courtesy of Fortec Motorsports).

The effect of a kerb impact on handling and vehicle stability can also be simulated by means of a step input on one of the front wheels followed by the same input on the same side rear wheel, after a time delay inversely proportional to the vehicle speed considered for the test. An overall performance index is generated by combining the 5 indexes above plus the kerb strike results, each one with a specific weight. Figure 1 shows a series of runs conducted in sequence and the overall performance index for each one of them. Each run (showed in the x axis) is performed with a different car configuration. The lower the index the higher the performance on track. Some comments were removed for confidentiality.
Both proposals require non-linearities to be removed from suspension rates, either on the seven-post rig and eventually in a software simulation environment, thus resulting in a theoretically optimum setup which is scarcely applicable to a real-world, race track setup, as already stated.
During a full championship season, as a matter of fact a race car is used on many different circuits, each one requiring a specific car configuration to improve lap time: both suspension and aerodynamics settings change form circuit to circuit and even from session to session. Table 1 below shows some circuit data and highlights their peculiarities.

Table 1. Circuit data.

Circuit	Aerodynmic configuration	Track roughness level	# turns	Speed (Km/h)			
				min	med	max	avg min at apex
circuit 1	High downforce	high	6	56	154	216	108
circuit 2	High downforce	low	11	80	158	224	122
circuit 3	High downforce	low	9	66	166	238	93
circuit 4	High downforce	low	11	80	165	225	123
circuit 5	Medium downforce	medium	12	62	170	245	115
circuit 6	Low downforce	medium	13	63	184	241	136

1.2. Proposal of a novel performance index
While the current industry approach tries to find a generic optimum for the suspension configuration without
any use of circuit-specific information, the index proposed in this work is aimed at representing race car road holding performance in terms of vertical dynamics in the frequency domain, including some of the non-linear effects that are usually neglected.
Downforce is proportional to vehicle speed squared and generates suspension deflection. Two kinds of non-linearity should be considered: the suspension stiffness is a function of suspension deflection because of the above-mentioned non-linear suspension rates and on top of this, downforce is a function of front and rear ride heights according to the so-called aeromaps, as explained in Section 2.2. This means in turn that suspension stiffness is related to vehicle speed through suspension deflection and aerodynamic properties.
The aerodynamic forces will be modelled using the induced angle of attack approach [18, 25, 34], where the angle of attack is a function of the vehicle body attitude and also of the bounce and pitch velocity. When the vehicle is bouncing, it creates an induced angle of attack proportional to bounce velocity. With pitch oscillation, the same happens. Using the induced angle of attack in the calculation of aerodynamic forces and moments, they become proportional to bounce and pitch velocities resulting in aerodynamic damping in bounce and pitch oscillations.
To calculate this novel index, the race car model is linearized for several values of longitudinal speed within a specific range, and the frequency response is plotted for each one of these speed values. The frequency response will change because the system stiffness and damping will change with vehicle longitudinal speed. This paper aims at showing that by means of these curves it is possible to evaluate a performance index representing the system road holding performance, thus improving the current approach results to achieve a circuit dependent optimum setup.

In this work the word “race car” refers to single seaters (from F4 up to F1). The results are based on a Formula 3 car. All vehicle data sets came from measurements and are courtesy of Fortec motorsports. They were validated for application purposes and also used in a previous work [20].

2. Methods

2.1. Vehicle model

The half car model is a classic model used in vehicle dynamics to evaluate vehicle comfort (through the estimate of vehicle body accelerations) and road holding (through evaluation of tyre contact patch load variations). The model features four degrees of freedom: sprung mass pitch and bounce, and front and rear unsprung mass vertical displacements, see Figure 2.

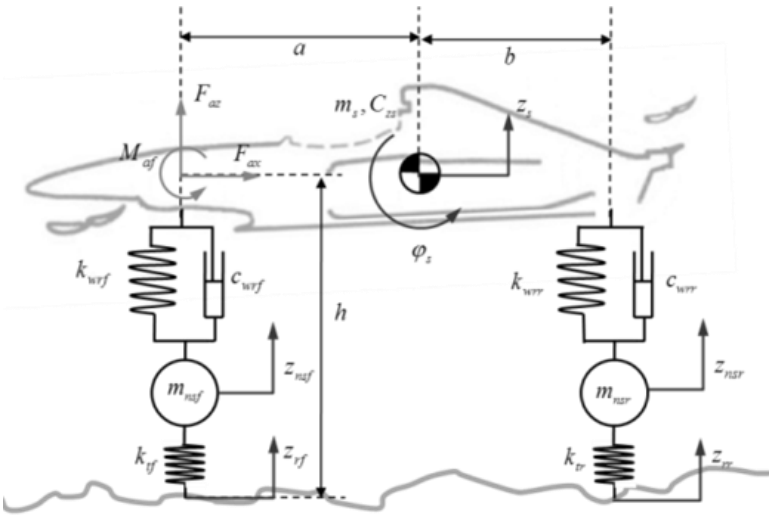

Figure 2. Half car model.

The aerodynamic actions are divided into downforce and pitch moment on the vehicle body. The reference for the aerodynamic forces is lying on the ground and aligned with the front axle. Equations (1), (2), (3) and (4) are the equations of motion. Equations (5) and (6) compute the tyre contact load while equation (7) compute the time delay between front and rear axle inputs.

$$I_y.\ddot{\alpha}_{ns} = F_a + a.F_a + F_{spring\,f}.a + F_{spring\,r}.b + c_{wf}\left(-\dot{z}_s + \dot{\varphi}_s.a + \dot{z}_{nsf}\right).a + \\ + c_{wr}(\dot{z}_{nsr} - \dot{z}_s - \dot{\varphi}_s.b).b \quad (1)$$

$$m_s.\ddot{z}_s = -F_a + F_{spring\,f} + F_{spring\,r} + c_{wf}\left(\dot{z}_s - \dot{\varphi}_s.a - \dot{z}_{nsf}\right) + c_{wr}(\dot{z}_{nsr} - \dot{z}_s - \dot{\varphi}_s.b) \quad (2)$$

$$m_{nsf}.\ddot{z}_{nsf} = F_{spring\,f} + c_{wf}\left(\dot{z}_s - \dot{\varphi}_s.a - \dot{z}_{nsf}\right) + k_{tf}\left(z_{rf} - z_{nsf}\right) \quad (3)$$

$$m_{nsr}.\ddot{z}_{nsr} = F_{spring\,r} + c_{wr}(\dot{z}_{nsr} - \dot{z}_s - \dot{\varphi}_s.b) + k_{tr}(z_{rr} - z_{nsr}) \quad (4)$$

$$F_{cf} = k_{tf}\left(z_{rf} - z_{nsf}\right) \quad (5)$$

$$F_{cr} = k_{tr}(z_{rr} - z_{nsr}) \quad (6)$$

$$z_{rr}(t) = z_{rf}\left(t - \frac{L}{V}\right) \quad (7)$$

Aerodynamic forces as well as wheel rates (i.e. suspension stiffness curves) are non-linear in the model. Downforce is non-linear mainly because of the interaction with the ground, the so-called ground effect. The wheel rates are non-linear in order to resist the high aerodynamic loads at high vehicle speed. Formulations for both actions are presented below.

2.2. Aerodynamic forces

In order to include the ground effect in the aerodynamic forces and moments, the vehicle ride height is included in the formulation. The non-linear relationships between forces and front and rear ride heights are expressed by the so-called aeromap surfaces. Figure 3 presents typical aeromap shapes for overall downforce (left) and aerobalance (right) derived from wind tunnel tests (values are related to a reference position due to a specific non-disclosure agreement). Both are functions of either front and rear ride height. The non-linear aerodynamic forces and coefficients are presented in equations (8) and (9) and are based on formulations used in other works [32] and by the industry [33].

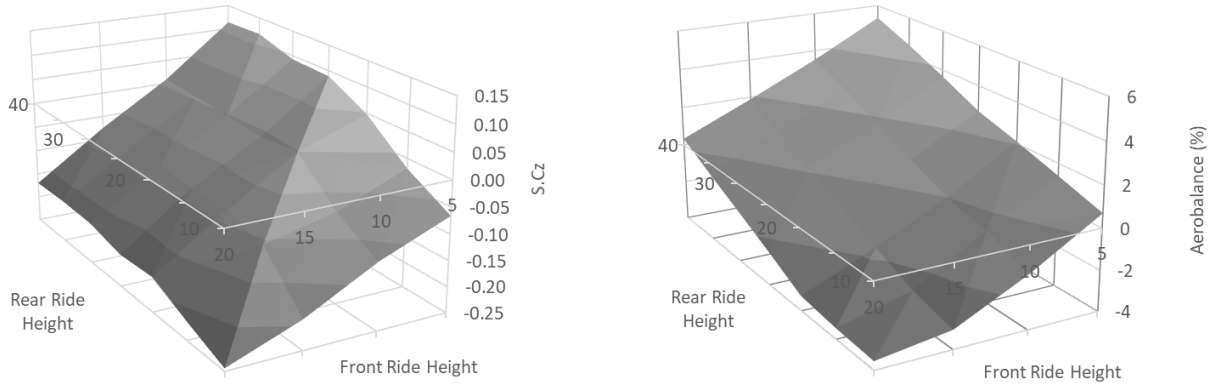

Figure 3. Typical aeromaps shape.

$$F_a = \frac{1}{2}\rho S C_z V^2 = pSC_z = pS\left(C_{z0} + \frac{\partial C_z}{\partial h_f}h_f + \frac{\partial C_z}{\partial h_r}h_r + \frac{\partial^2 C_z}{\partial h_f^2}h_f^2 + \frac{\partial^2 C_z}{\partial h_r^2}h_r^2 + \frac{\partial^2 C_z}{\partial h_f \partial h_r}h_f h_r\right) \quad (8)$$

$$M_a = \frac{1}{2}\rho S C_m L V^2 = pL\left(C_{m0} + \frac{\partial C_m}{\partial h_f}h_f + \frac{\partial C_m}{\partial h_r}h_r + \frac{\partial^2 C_m}{\partial h_f^2}h_f^2 + \frac{\partial^2 C_m}{\partial h_r^2}h_r^2 + \frac{\partial^2 C_m}{\partial h_f \partial h_r}h_f h_r\right) \quad (9)$$

The front and rear ride heights in equations (8) and (9) are replaced by equations (10) and (11), as both are a function of centre of mass displacement and pitch angle.

$$h_f = z_s + \varphi_s a \quad (10)$$

$$h_r = z_s - \varphi_s b \quad (11)$$

Replacing equations (10) and (11) into equation (8), the downforce can be calculated as presented in equation (12) and the pitch moment coefficient can be calculated in the same way.

$$C_z = C_{z0} + \frac{\partial C_z}{\partial z}z + \frac{\partial C_z}{\partial \varphi}\varphi + \frac{\partial^2 C_z}{\partial z^2}z^2 + \frac{\partial^2 C_z}{\partial \varphi^2}\varphi^2 + \frac{\partial^2 C_z}{\partial z \partial \varphi}z\varphi \quad (12)$$

In the transient calculations the model is linearized for a specific value of vehicle longitudinal speed. Equations (13) and (14) present the linearized aerodynamic coefficients.

$$C_{z(v)} = C_{z\,base} + \frac{\partial C_z}{\partial \varphi}_{(v)}\varphi + \frac{\partial C_z}{\partial z}_{(v)}z \quad (13)$$

$$\frac{\partial C_z}{\partial \varphi}_{(v)} = \frac{\partial C_z}{\partial \varphi} + 2\frac{\partial^2 C_z}{\partial \varphi^2}\varphi + \frac{\partial^2 C_z}{\partial z \partial \varphi}z \quad (14)$$

The aerodynamic model formulation follows the approach adopted by other authors that work with unsteady aerodynamics in ground effect [34, 35]. They showed that three main effects are important for unsteady aerodynamics: the ground clearance, the induced angle of attack and the added mass. These effects are related to bounce displacement, velocity and acceleration respectively. Each one of these effects works in a specific range of frequency [36]. In this work the effect of added mass will be neglected as it affects high frequencies only and in the proposed work the model will be limited to

inputs up to 60 Hz. This limit assures that the sprung and unsprung mass natural frequencies will be covered.
The pitch angle used in the computation of aerodynamic forces and moments will be a function of pitch displacement and velocity, and bounce velocity, as presented in equation (15). In the aerospace industry this approach is known as induced angle of attack.

$$\varphi = \varphi_s + \dot{\varphi}_s \frac{L}{V} + \frac{\dot{z}_s}{V} \tag{15}$$

Equation (16) presents the aerodynamic downforce coefficients linearized for a fixed vehicle longitudinal speed and with the effect of the induced angle of attack as shown in equation (15).

$$C_z = C_{z\,0} + \left(\frac{\partial C_z}{\partial z}_{(v)} a + \frac{\partial C_z}{\partial \varphi}_{(v)}\right)\varphi_s + \left(\frac{\partial C_z}{\partial z}_{(v)}\right) z_s + \left(\frac{\partial C_z}{\partial \varphi}_{(v)} \frac{1}{V}\right)\dot{z}_s + \left(\frac{\partial C_z}{\partial \varphi}_{(v)} \frac{L}{V}\right)\dot{\varphi}_s \tag{16}$$

2.3. Spring and bump stop forces
In order to include the non-linear effects of the bump stop, a non-linear stiffness curve was used. This force can be modelled using a lookup table. In the linearized model, the stiffness was calculated in the operation point. The bump stop hysteresis has been neglected as it is smaller compared to damper forces.
The bump stop is not always being compressed: the static gap between the bump stop itself and the damper body is used to set its initial position, as showed in Figure 4. Equation (17) presents how the spring and bumpstop forces were implemented.

$$\mathrm{F} = \mathrm{K}.\mathrm{x} + f(\mathrm{x} - \mathrm{gap}) \tag{17}$$

3. Results and discussion

3.1. Quasi-static
The quasi-static calculations were conducted by applying a vehicle longitudinal speed sweep from 0 to 230 km/h, therefore neglecting any longitudinal acceleration. This is a common procedure to understand how ride heights evolve as a function of vehicle speed and to set static ride heights and bump stop gaps for a specific circuit. This procedure is also used to validate the suspension deflection with aerodynamic load. Figure 4 shows a comparison between the model and track data for circuit 2.

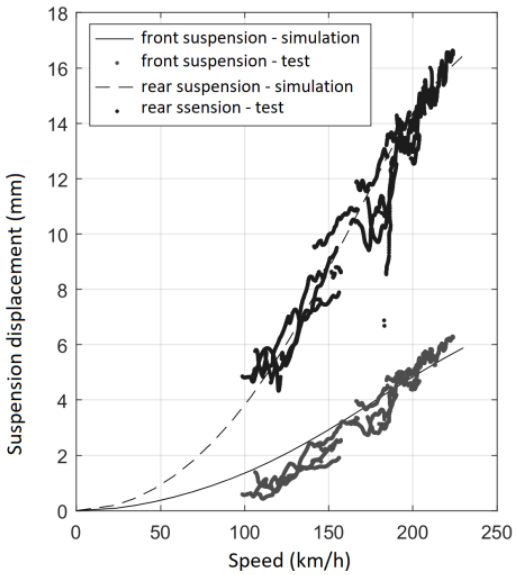

Figure 4. Suspension deflection due to aerodynamic forces.

Race cars must have their suspension set to maximize vehicle performance on track. This implies that the car ground clearance should be as low as possible. As vehicle longitudinal speed increases suspensions and tyres are compressed by increasing downforce, and ground clearance is therefore reduced. At first glance, the key point is to set the race car not to touch the ground and because of that the suspension stiffness should be high enough. Therefore, bump stops are normally used to achieve a rising rate. The key variables in quasi-static vertical dynamics are called dynamic ride heights: they are the front and rear ride heights as a function of vehicle longitudinal speed, as shown in Figure 5.

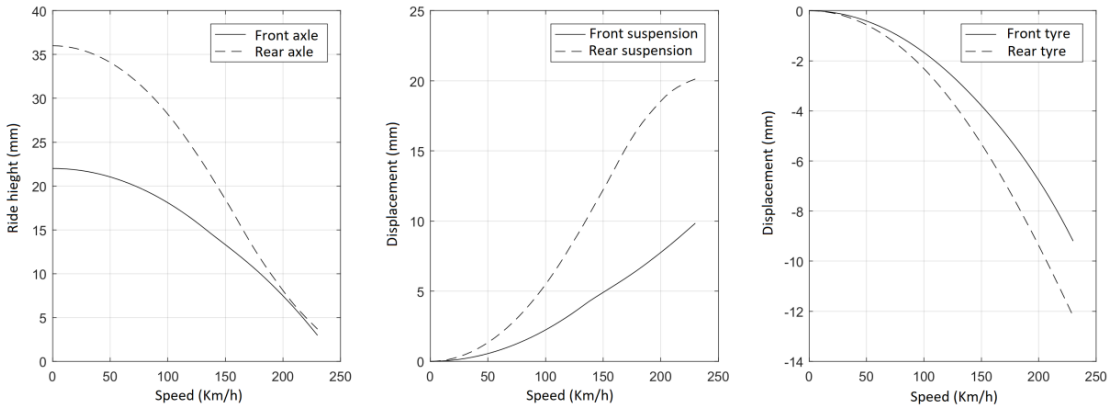

Figure 5. Dynamic ride heights, suspension displacement and tyre deflection against vehicle longitudinal speed.

On the left of Figure 5 the dynamic ride height vs vehicle speed curves show that the rear suspension features a visible change in stiffness while the front is smoother. This happens because the rear bump stop stiffness is much higher than the spring stiffness. The front bump stop gap is 3 mm while the rear is 6 mm. The front bump stop is engaged at around 130 km/h and the rear one around 160 km/h.
Formula cars generally use fairly wide tyres with a high aspect ratio due to the mandatory use of 13" rims. Because of that, their radial stiffness is relatively low with respect to a road car tyre. As a matter of fact, the suspension/tyre stiffness ratio can be as low as 1:1 (a typical road car stiffness ratio is about 1:10). When the bump stops come into play at high vehicle longitudinal speed the suspension can get nearly solid, creating a system with awkward dynamics when compared to a road car. Whenever tyre stiffness is smaller than suspension stiffness it dominates the dynamic response, leaving the system almost undamped. In Figure 5 at maximum vehicle speed, the overall ride height drop at the front is about 19 mm; tyre radial deflection accounts for about 50%. The rear ride height drop is about 32 mm, of which 37.5% is due to tyre deflection. This is common practice for a typical single seater: the front suspension is set to be much stiffer than the rear.

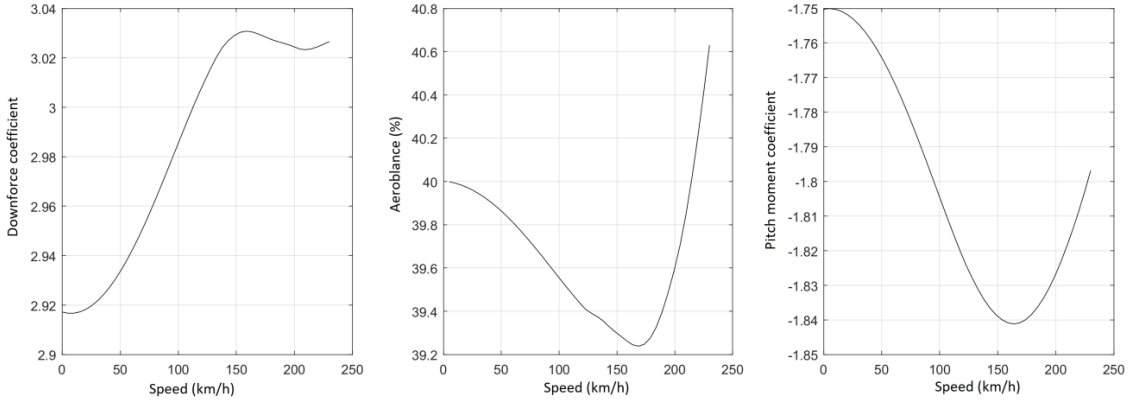

Figure 6. Aero parameters as a function of vehicle speed.

As stated above the dynamic ride heights have a direct impact on the so-called ground effect and heavily affect aerodynamic performance. As the aerodynamic coefficients are a function of both front and rear ride heights, setting the correct dynamic ride heights for a given circuit is vital for performance. Figure 6 is based on the so-called vehicle aeromaps and shows the downforce, aerobalance and pitch moment coefficients as a function of vehicle longitudinal speed. The drop of downforce above 150 km/h is peculiar of a single seater aerodynamic behaviour and it is due to diffuser stall: it happens when the rear ride height becomes low and it is mainly due to the boundary layer. This drop of downforce also results in a drop of aerodynamic drag; hence it is desirable in order to increase vehicle top speed at the end of a long straight.

3.2. Transient

Race car vertical dynamics is a compromise between aerodynamic stability and road holding. The first one is about the longitudinal movement of the centre of pressure and the second one has been explained above. When vehicle speed increases, chassis ground clearance and suspension stiffness change, and vehicle frequency response changes as a consequence.

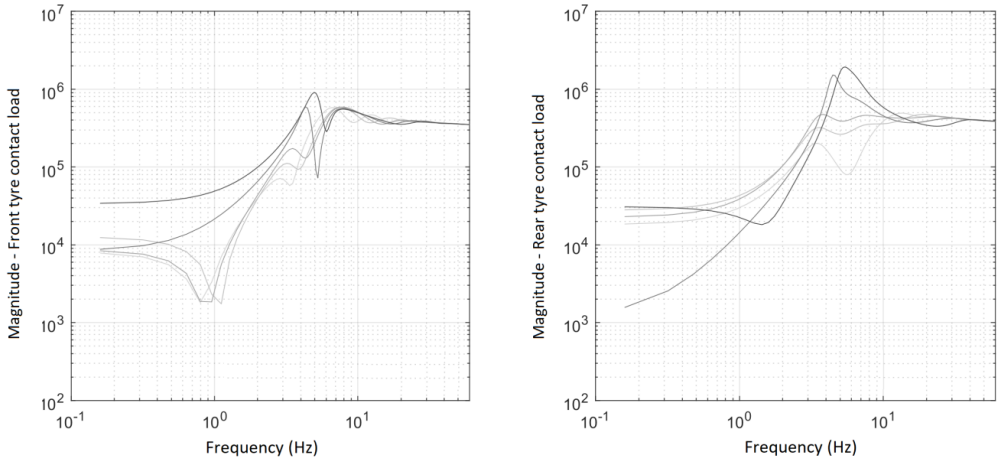

Figure 7. Tyre contact load frequency response (higher vehicle speeds in darker colours).

The equations of motion presented before were linearized for a range of vehicle speed values (from 0 up to 230 km/h) and transformed into a system of first-order differential equations presented in equation (18). Contact patch load variation for front and rear axles are calculated as outputs as shown in equation (19). As matrix A is not diagonal the pitch and bounce vibration modes are coupled [37]. The rear tyre input was modelled with a time delay as a function of vehicle speed and wheelbase length, see last item of equation (18) and equation (19). The frequency response from 0 up to 230 km/h for a Formula 3 car was obtained by deriving the equations above. Figure 7 shows the tyre contact load frequency response when the model is linearized at 5 different vehicle speed values: its shape is strongly related to vehicle speed because of the wheelbase filtering effect, the suspension rising rate, the relationship between aerodynamic actions and ride heights and the induced angle of attack.

$$\begin{bmatrix} \dot{z}_s \\ \dot{\alpha}_s \\ \dot{z}_{nsf} \\ \dot{z}_{nsr} \\ \dot{\omega}_s \\ \dot{v}_s \\ \dot{v}_{nsf} \\ \dot{v}_{nsr} \end{bmatrix} = \mathbf{A}. \begin{bmatrix} z_s \\ \alpha_s \\ z_{nsf} \\ z_{nsr} \\ \omega_s \\ v_s \\ v_{nsf} \\ v_{nsr} \end{bmatrix} + \begin{bmatrix} 0 \\ 0 \\ 0 \\ 0 \\ 0 \\ 1 \\ 0 \end{bmatrix} . \mathrm{u}(t) + \begin{bmatrix} 0 \\ 0 \\ 0 \\ 0 \\ 0 \\ 0 \\ 1 \end{bmatrix} . \mathrm{u}(t-\tau) \tag{18}$$

$$\begin{bmatrix} Fc_f \\ Fc_r \end{bmatrix} = \begin{bmatrix} 0 & 0 & -K_{tf} & 0 & 0 & 0 & 0 & 0 \\ 0 & 0 & 0 & -K_{tr} & 0 & 0 & 0 & 0 \end{bmatrix} \boldsymbol{x} + \begin{bmatrix} K_{tf} \\ 0 \end{bmatrix} \mathrm{u}(t) + \begin{bmatrix} 0 \\ K_{tr} \end{bmatrix} \mathrm{u}(t-\tau) \quad (19)$$

4. The Road Holding Performance Index (RHPI)

The proposed performance index is calculated using the contact load frequency response, a track profile density function and a vehicle speed range (from 0 up to 230 km/h in steps of 5 km/h in the present case). The contact load frequency response is multiplied by a track profile density function, and the results (inertance) are integrated over a frequency range of 0.1 Hz up to 60 Hz, generating the contact load RMS value for each vehicle speed value. The integral of the RMS values over a vehicle speed range (circuit dependent) generates the proposed index. The calculation process is explained in the chart below (Figure 8).

To evaluate the vehicle vertical time response attributable to excitation by pavement irregularities, the convolution of the vehicle function with the surface vertical displacement profile can be used [37]. However, in the frequency domain, the spectral response may be obtained directly only by multiplying the spectrum of the two systems. The resulting function is the inertance magnification of vehicle contact load attributable to spectral pavement roughness.

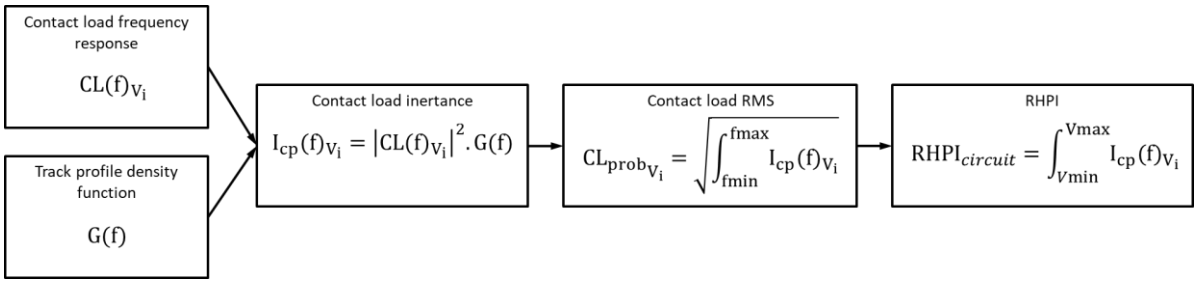

Figure 8. Block diagram representing the index calculation steps.

In this work, the proposed performance index was calculated for a mathematical road profile compatible to standard asphalt type "C" [38]. The Figure 9 presents the contact load inertance. By integrating the inertance function in the frequency range it is possible to plot the contact load RMS as a function of vehicle speed.

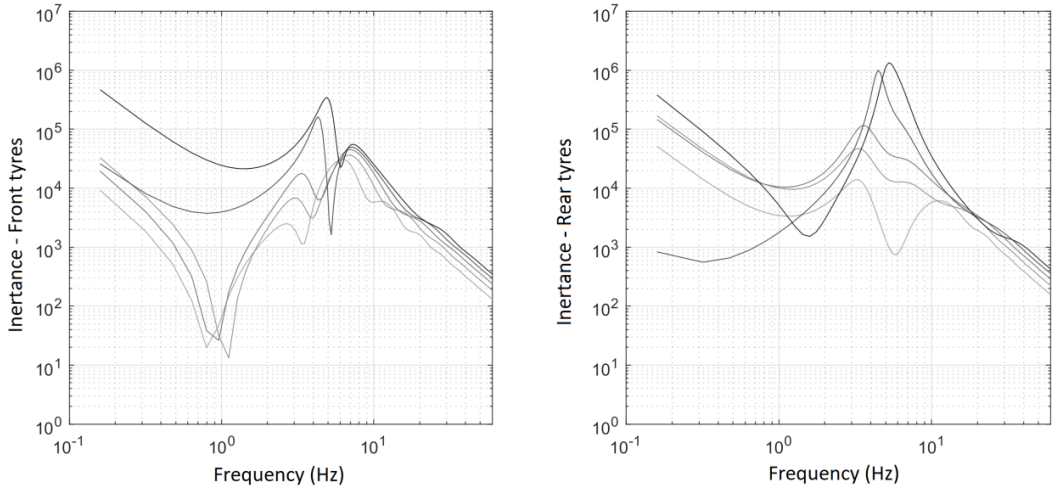

Figure 9. Contact load inertance function for front and rear tyres (higher vehicle speeds in darker colours).

Figure 9 shows the contact load inertance for the front and rear tyres. The track profile amplifies the low frequency and reduces the high frequency gains from the contact load frequency response (Figure 7).

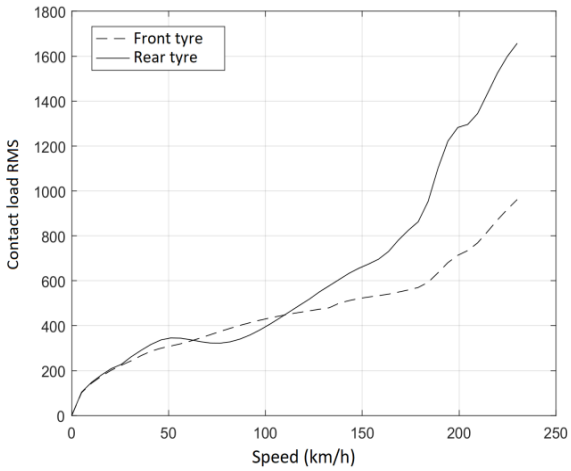

Figure 10. Tyre contact patch load RMS vs. vehicle speed.

The integral of the contact load inertance (contact load RMS) at each vehicle longitudinal speed value is presented in Figure 11: low values correspond to better road holding behaviour. Any change in car settings (spring stiffness, etc.) will also change this curve. Each circuit presented in Table 1 force the vehicle to work in a specific vehicle speed range. This means that the values in Figure 10 can be windowed for each circuit speed range. The non-linearities are due to the changes in system stiffness and damping. The front bump stop starts to be compressed at around 130 km/h and the rear around 160 km/h.

Figure 11 shows a sensitivity check of the contact load RMS for different race car settings. The influence of front and rear static ride heights is presented in the first column. The second column shows the influence of front and rear bump stop gaps. The third column presents the effects of a change in terms of aerobalance (i.e. the position of the centre of pressure, on top) and a of a suspension rate variation (front and rear). The latter basically compares a "stiff" setup for a smooth track surface with a "soft" setup designed to cope with the bumps of a street circuit.

Although small, a change of the performance index is clearly visible in all cases. It is important to remember that race car performance is often measured in tenths or even hundredths of a second.

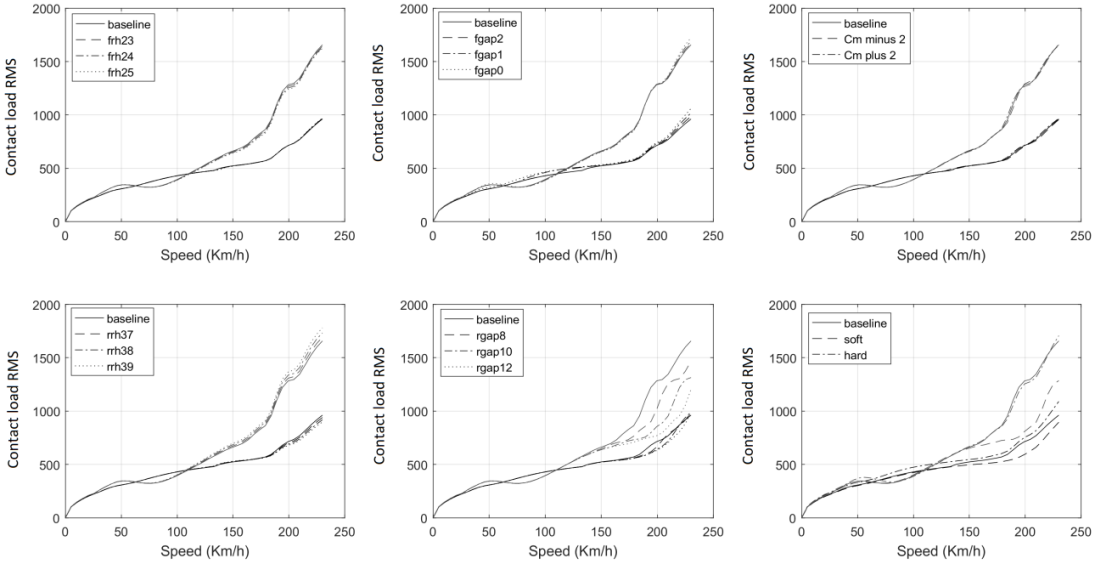

Figure 11. Sensitivity of the contact load RMS: from left to right, effects of front and rear static ride heights (frh and rrh respectively); effects of front and rear static bump stop gaps (fgap and rgap); effects of aerobalance variation and suspension rate (softer vs harder).

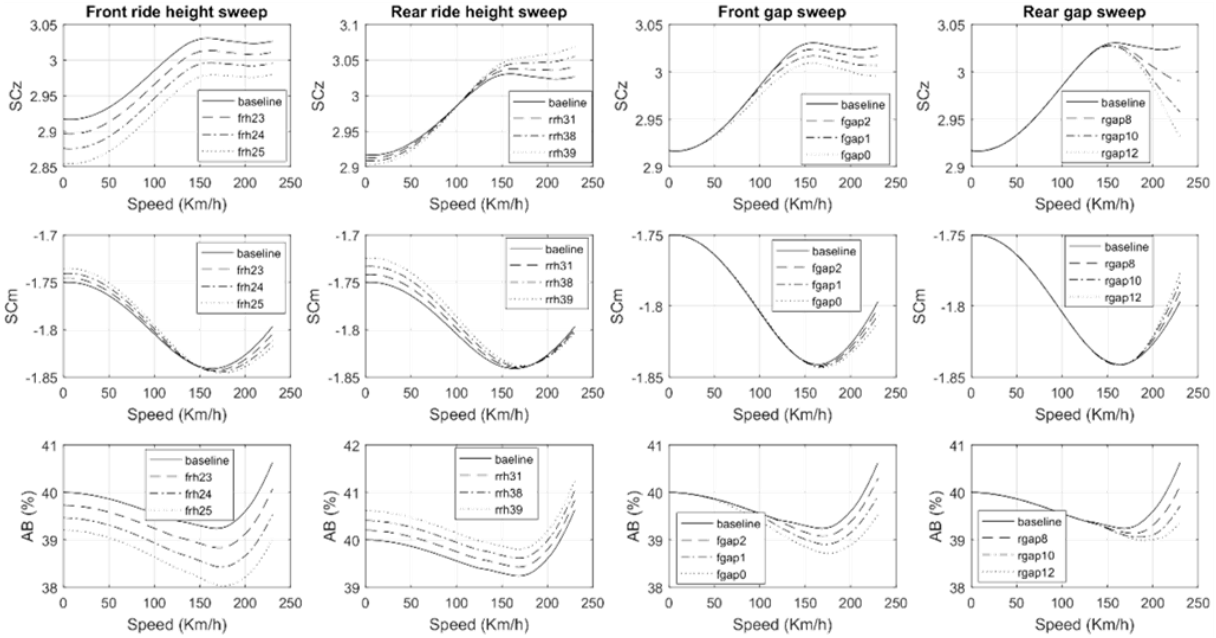

Figure 12. Influence of the simulated suspension settings on aerodynamic coefficients.

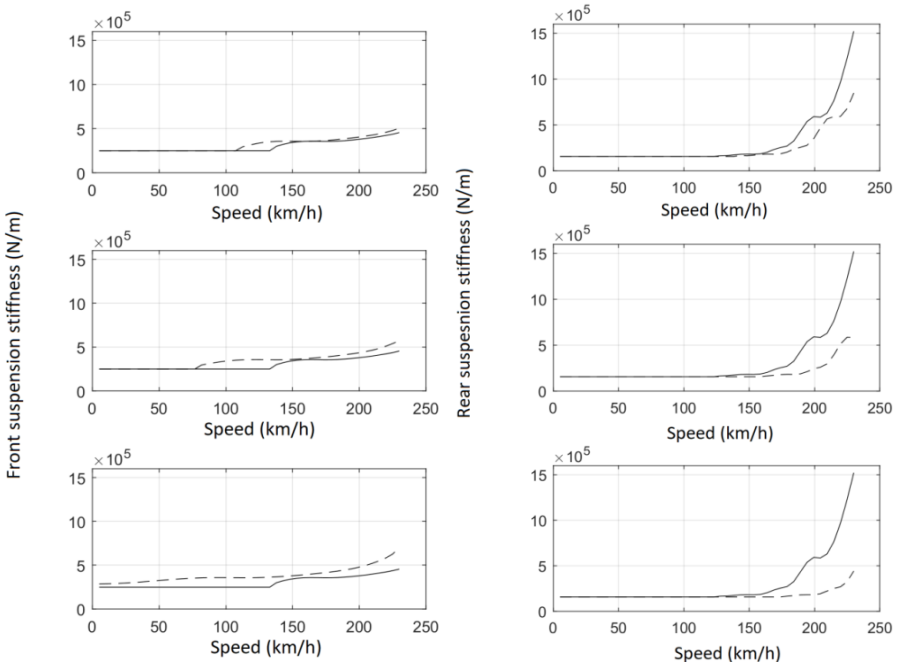

Figure 13. Suspension stiffness vs vehicle longitudinal speed. Bump stop gap changes as in third and fourth columns of Figure 12.

Figure 11 suggests that sensitivity of the rear axle is usually more visible than the front one for all changes made. The main factor is the rear bump-stop gap. It also shows how different setup settings in terms of suspension rate can have a big impact on the curves.

Figure 12 shows how the aerodynamic coefficients are influenced by the suspension changes presented in the first and second columns of Figure 11 (front and rear static ride heights and bump stop gaps). Any variation of the rear bump stop gap has the largest effect on aerodynamic forces, and consequently on the rear tyre contact patch loads (Figure 11). This is an effect of the change in terms

of dynamic ride heights due to the bump stops and to the non-linear relationship between aerodynamic forces and ride heights.
Figure 13 shows how the static bump stop gaps affect suspension stiffness: front bump stop gap in the left column, rear gap in the right. The dashed line is the baseline while the solid line is the modified setup. Although the gap steps in millimetres are the same, the rear is more sensitive to changes as the bump stop/spring stiffness ratio is higher than the front.
Finally, the integral of the tyre contact patch load RMS versus vehicle longitudinal speed (Figure 10), gated for a speed range of a target circuit (the example shows circuit 1 and circuit 2) represents the proposed Road Holding Performance Index (RHPI), summarizing the road holding behaviour in a single, RMS-based number. Higher values represent high tyre contact patch load variation, meaning less performance. Figure 14 shows the effect of various setup changes on the RHPI for the front and rear axles as well as the front/rear average RHPI as a representative index for the complete vehicle. These plots show that a different vehicle speed range (different circuits) will excite the system in a different way, consequently unsettling the contact patch load in different magnitudes. Once more, the biggest changes are related to the rear suspension gap, as this will change rear suspension stiffness and move the onset of rear diffuser stall to a different vehicle speed as well (Figure 12).

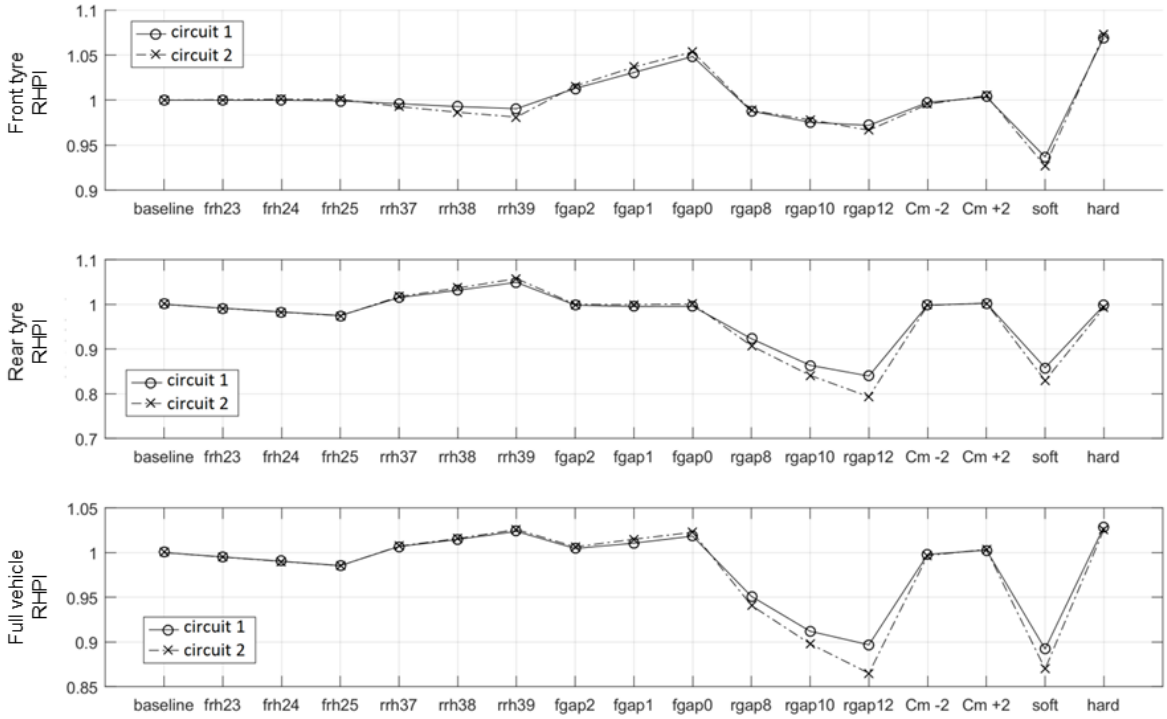

Figure 14. Road Holding Performance index for different car settings and for circuits 1 and 2.

5. Conclusion

The paper proposes a Road Holding Performance Index including several racecar parameters that are not commonly used in the literature and by the industry.
Aerodynamic forces change vehicle stiffness progressively as speed increases. Suspension stiffness non-linearities are important to control ground clearance and to keep the car within a proper ride height range (as shown in the quasi-static simulation); they also have a significant impact on vehicle system dynamics. The analysis of the system behaviour without these non-linearities would generate a vehicle setup that is impractical for circuit use or at least not fully realistic. The linearization as a function of vehicle longitudinal speed showed a very good correlation with typical racecar dynamics. The non-linear effects are clearly visible by means of the proposed performance index (Figure 14).

The performance index was calculated using numerical simulation, but it is also possible to generate it by means of the so-called four- or seven-post rig testing. This unprecedented approach would require further research.
Although the optimization of the transient response is important to improve racecar performance, setting suspension stiffness and static ride heights is a priority. The RHPI offers the opportunity to optimize the design of damping and spring rate characteristics by means of the traditional quasi-static analysis (Figure 5 and 6).
Further developments are possible by taking bump stop hysteresis into account and also by creating a new performance index coupling aerodynamic stability with vertical dynamics.

Symbols

a	distance from sprung mass center of gravity to front axle
AB	aerobalance
b	distance from sprung mass center of gravity to rear axle
c_i	weight factor
c_f	contact force index
C_m	pitch moment coefficient
C_{wr}	front damping coefficient at wheel
C_z	downforce coefficient
F_a	aerodynamic force
$F_{a\,mass}$	aerodynamic force due to added mass effect
F_{spring}	force at suspension spring
F_{wheel}	spring force at wheel
gap	spring deflection required to engage bump stop
h	ride height
K_{wr}	spring rate at wheel
L	wheelbase length
M_a	aerodynamic pitch moment
m_{ns}	unsprung mass
m_s	sprung mass
p	dynamic pressure
rh	ride height
S	vehicle reference frontal area
t	time
V	vehicle longitudinal speed
x_{spring}	spring displacement
x_{wheel}	relative displacement between wheel and sprung mass
z_{ns}	unsprung mass vertical displacement
z_r	road displacement input to the tyre
z_s	sprung mass vertical displacement
φ_s	sprung mass pitch angle
ρ	air density
ϑ	air volume displaced

Subscripts

0	static value
f	front
r	rear

Acknowledgments
The authors would like to thank Fortec Motorsports UK for all data supplied and their support.

References

[1] Chindamo, D.; Gadola, M.; Romano, M. (2014). Simulation tool for optimization and performance prediction of a generic hybrid electric series powertrain. International Journal of Automotive Technology, 15:135–144.
[2] Wright, P. Formula 1 Technology. 1st edition. SAE, 2001.
[3] Cecchel, S.; et al. (2018). Impact of reduced mass of light commercial vehicles on fuel consumption, CO2 emissions, air quality, and socio-economic costs. Science of the total environment. (613-614), 409-417.
[4] Cecchel, S.; et al. (2018). Lightweighting in automotive: cradle- to- grave life cycle assessment of a safety relevant component. International Journal of Life Cycle Assessment. 23(10), 2043-2054.
[5] Chindamo, D.; Gadola, M. (2018). What is the Most Representative Standard Driving Cycle to Estimate Diesel Emissions of a Light Commercial Vehicle? Proceedings of the 1st IFAC Workshop on Integrated Assessment Modelling for Environmental Systems, (IAMES 2018), May 2018, Brescia, Italy. IFAC-PapersOnLine, 51(5), 73-78.
[6] Reimpell, J.; Stoll, H.; Betzler, J. The Automotive Chassis: Engineering Principles. 2001, Second Edition, Butterworth Heinemann.
[7] Barcelo, J. D. P. (2012). Optimization of Racing Car Suspensions featuring Inerters. (PhD Thesis). Department of Mechanical Engineering and Mathematical Sciences, Oxford Brookes University.
[8] New, T. M. Random Road Analysis and Improved Gear Ratio Selection of a Front Wheel Drive Drag Racing Car. 2008. (MSc Thesis). Clemson University.
[9] Chindamo, D.; et al. (2017). Design of an indoor simulator for motorcycle applications. Applied Sciences. 7(12), 1220.
[10] Chindamo, D.; et al. (2017). BikeShake: the design of an indoor simulator dedicated to motorcycle ride testing as an interactive project. International Journal of Interactive Design and Manufacturing. (IJIDeM). 12(4), 1371-1383.
[11] Zhao, J.; et al.; Chassis integrated control for active suspension, active front steering and direct yaw moment systems using hierarchical strategy, Vehicle System Dynamics, 2017, 55(1), 72-103.
[12] Coric, M. et al.; Optimisation of active suspension control inputs for improved vehicle handling performance, Vehicle System Dynamics, 2017, 54 (1), 1574-1600.
[13] Benini, C.; et al. The influence of suspension components friction on race car vertical dynamics, Vehicle System Dynamics, 2017, 55 (3), 338-350.
[14] Matsubara, M. et al.; Natural frequency analysis of tyre vibration using a thin cylindrical shell model, SAE Technical Paper, SAE Noise and Vibration Conference and Exhibition; DeVos Place Convention CenterGrand Rapids; United States; 2015.
[15] Chindamo, D.; et al. (2018). On the vehicle sideslip angle estimation: a literature review of methods, models and innovations. Appl. Sci. 2018, 8(3), 355.
[16] Gadola, M.; Chindamo, D. (2018). Estimation of vehicle side-slip angle using an artificial neural network. MATEC Web of Conferences 166, 02001 - The 2nd International Conference on Mechanical, Aeronautical and Automotive Engineering (ICMAA 2018). Singapore, Feb 2018.
[17] Gadola, M.; et al. (2018). On the Passive Limited Slip Differential for High Performance Vehicle Applications. 14th International Symposium on Advanced Vehicle Control AVEC 18, Beijing, July 16-20 2018.
[18] Floyd, R.; Law, E. Simulation and Analysis of Suspension and Aerodynamic Interactions of Race Cars. Motorsport Engineering Conference & Exposition: SAE. SAE Paper 942537 1994.

[19] Kasprzak, JL.; Floyd, RS. Use of simulation to tune race car dampers. SAE Paper 942504, 1994.
[20] Marchesin, F.P: et al. (2017). High downforce racecar vertical dynamics: aerodynamic index. Vehicle System Dynamics, 56(8), 1269-1288.
[21] Dal Bianco, N.; et al. Minimum time optimal control of a GP2 race car. Proceedings of the Institution of Mechanical Engineers, Part D: Journal of Automobile Engineering. 2018, 232(9), 1180-1195.
[22] Doniselli, C.; et al. Aerodynamic Effects on Ride Comfort and Road Holding of Automobiles. Vehicle System Dynamics, v. Supplement 25, 1996.
[23] Kelly, J.; Kowalczyk, H.; Oral, H. Track Simulation and Vehicle Characterization with 7 Post Testing. Motorsport Engineering Conference & Exhibition, 2002, SAE.
[24] Kowalczyk, H. Damper tuning with use of a seven-post shaker rig. SAE 2002 World Congress. Detroit Michigan.
[25] Cambiaghi, D.; Gadola, M.; Vetturi, D. Suspension System Testing and Tuning with the Use of a Four-Post Rig. SAE 1998.
[26] Chindamo D.; et al. Reproduction of real-world road profiles on a four-poster rig for indoor vehicle chassis and suspension durability testing. Advances in Mechanical Engineering, Vol (9)8, 2017.
[27] MTS, RPC Pro Software, 2014 MTS Corporation
[28] Marchesin, et al. (2016). Upright mounted pushrod: the effects on racecar handling dynamics. The Dynamics of Vehicles on Roads and Tracks. Proceedings of the 24th Symposium of the International Association for Vehicle System Dynamics, IAVSD 2015. (10), 543-552.
[29] Crema, C.; et al. (2015). Smartphone-based system for vital parameters and stress conditions monitoring for non-professional racecar drivers. Proceedings of the 2015 IEEE SENSORS. 7370521.
[30] Multimatic. A note in the use of four post test rigs. p.20. 1998
[31] Fung,Y.C., An Introduction to the Theory of Aeroelasticity, Dover Publications, 2008
[32] Mavroudakis, B. About the simulations of Formula 1 Racing Cars. 2010. Institute of Engineering and Computational Mechanics, University of Stuttgart
[33] Dallara, Formula Renault 3.5 2012 Aerobook, release 1.1, Dallara Automobili 2012
[34] Fuller, J., et al., The importance of unsteady aerodynamics to road vehicle dynamics, Journal of Wind Engineering and Industrial Aerodynamics, 2013, vol. 117, 1-10.
[35] Molina J.; Zhang, Z.; Arodynamics of a heaving airfoil in ground effect, AIAA Journal, Vol. 49, No. 6, 2011
[36] Barbosa, RS.; Vehicle Dynamic Safety in Measured Rough Pavement. Journal of Transportation, 2011
[37] Newland, D. E. (1984). An introduction to random vibrations and spectral analysis, 2nd Ed., Longman Scientific & Technical, New York, 377.
[38] AASHTO (2001). Standard Specifications for Transportation Materials and Methods of Sampling and Testing. Standard TP 62-03, Standard Method of Test for Determining Dynamic Modulus of Hot Mix Asphalt Concrete Mixtures, Washington, DC.